coatings

MDPI

Article

Preparation and Characterization of the Cr-Nanodiamonds/MoN Coatings with Performant Mechanical Properties

Vadzim Chayeuski [1], Abdelhafed Taleb [2,3,*], Valery Zhylinski [4], Andrei Kuleshov [5] and Roman Shtempliuk [6]

[1] Department of Physics, Faculty of Information Technology, Belarusian State Technological University, 13a, Sverdlov Street, 220006 Minsk, Belarus; chaevskiv@gmail.com
[2] Chimie ParisTech, PSL University, CNRS, IRCP, 75005 Paris, France
[3] Sorbonne Université, 4 Place Jussieu, 75231 Paris, France
[4] Department of Chemistry, Technology of Electrochemical Production and Electronic Engineering Materials, Chemical Technology and Engineering Faculty, Belarusian State Technological University, 13a, Sverdlov Street, 220006 Minsk, Belarus; zhilinski@yandex.ru
[5] Department of Solid State Physics, Faculty of Physics, Belarusian State University, 4, Nezavisimosti Avenue, 220030 Minsk, Belarus; kuleshak@bsu.by
[6] The Joint Institute of Mechanical Engineering of the NAS of Belarus, 12, Akademicheskaya Street, 220072 Minsk, Belarus; sintaby92@gmail.com
* Correspondence: abdelhafed.taleb@sorbonne-universite.fr; Tel.: +33-(1)-85-78-41-97

Abstract: This paper presents the results of a study on the preparation and characterization of a Cr-DND/MoN detonation chromium-nanodiamond coating deposited on cemented tungsten carbide (WC–3 wt.% Co) mill blades using Arc-PVD and electrodeposition methods. The physical and mechanical characteristics of the coatings were investigated by scanning electron microscopy (SEM), energy dispersive X-ray spectroscopy (EDS), XRD analysis, Raman spectroscopy, micro-identification, and scratch test (evaluation of the coating adhesion). It was shown that the Cr-DND/MoN coating consists of successive layers of Cr-DND (top), Cu (middle) and MoN (bottom) with separate phases of γ-Mo_2N, α-Mo, α-Cu, Cr-DND and nanodiamonds. The Cr-DND composite electrochemical coating (CEC) was deposited from the conventional chromium plating electrolyte with the addition of nanodiamonds. The copper interlayer was deposited by the Arc-PVD method on the surface of the MoN coating to improve the adhesion strength of the Cr-DND CEC. The coating showed an optimum microhardness of about 14 ± 1 GPa and good adhesion with a critical load L_c of about 93 N. In addition to the expected experimental results, the coating has high wear resistance, confirmed by scratch tests.

Keywords: coating; nanodiamonds; chromium; molybdenum nitride; mechanical properties

check for updates

Citation: Chayeuski, V.; Taleb, A.; Zhylinski, V.; Kuleshov, A.; Shtempliuk, R. Preparation and Characterization of the Cr-Nanodiamonds/MoN Coatings with Performant Mechanical Properties. *Coatings* **2022**, *12*, 1012. https://doi.org/10.3390/coatings12071012

Academic Editor: Heping Li

Received: 28 June 2022
Accepted: 13 July 2022
Published: 18 July 2022

Publisher's Note: MDPI stays neutral with regard to jurisdictional claims in published maps and institutional affiliations.

Copyright: © 2022 by the authors. Licensee MDPI, Basel, Switzerland. This article is an open access article distributed under the terms and conditions of the Creative Commons Attribution (CC BY) license (https://creativecommons.org/licenses/by/4.0/).

1. Introduction

The world's leading tooling companies (Leitz, TIGRA, LEUCO, KANEFUSA CORPORATION, Iscar, Sandvik Coromant, etc.) have been using innovative materials in recent years to create commercial products, paying great attention to the development of new hard alloys and high-speed steels [1–4]. Milling cutters with WC-Co cemented carbide are widely used to process materials [5,6]. Although these tools offer a good ratio of hardness to crack resistance in woodworking [7], they cannot fully meet the requirements of modern wood processing due to the corrosion of cemented carbides [8–10]. In addition to the synthesis of new materials, research is being carried out to protect the surface layers of such tools against wear and to preserve their geometry under increasingly demanding processing conditions [11]. One of the main directions of this activity is the development and use of wear-resistant coatings on cutting tools. It has already been shown that coatings, unlike other methods of hardening the surfaces of construction materials, can increase tool productivity and improve the quality of the treated surface [12,13].

Today, one of the most common methods of material design is to create multilayer coatings composed of layers of different compositions using cathodic vacuum physical vapor deposition (Arc-PVD) on milling cutters [14–16]. The deposition of multilayer composites increases stability against external influences [17,18]. It has been reported in the literature that a multilayer Si-$MoSi_2$ coating structure consisting of molybdenum can improve the thermal resistance, corrosion resistance and mechanical properties of a coating [19,20]. Combinations of chromium and molybdenum nitrides have been shown to have the best characteristics [21–23].

In addition, the method of co-deposition of dispersed particles with metal coatings results in composite electrochemical coatings (CECs) with increased hardness, corrosion resistance and wear resistance, and low friction [24].

The deposition of diamond coatings on WC-Co cemented carbide cutters of cutting tools by chemical vapor deposition (CVD) is reported in [25,26]. Diamonds with a characteristic size of a few to several hundred nanometers are known as nanodiamonds or ultra-dispersed diamonds (UDD) [27]. Various methods have been used for the synthesis of nanodiamonds, including synthesis at high pressures and temperatures [28], chemical vapor deposition (CVD), laser ablation [29], detonation synthesis [30], etc. Of these methods for synthesizing nanodiamonds, only detonation synthesis is used on an industrial scale (several tens of tonnes per year) because of its speed, relative simplicity and low cost for large quantities. An industrial line for the production of nanodiamonds by detonation synthesis (DND) with pressurized nitric acid at temperatures of 200–250 °C is part of the FSUE "SCTB "Technology" (St. Petersburg) facility [31]. In Belarus, they are produced at JSC "Sinta" (Minsk) [32].

DND is used in the creation of CECs, polymer compositions, lubricants, polishing pastes, etc. [33,34]. Modification of chromium coatings with DND improves their tribomechanical properties, reducing the coefficient of friction for lubrication-free conditions by 1.8 to 2.9 times and the wear intensity by 6 to 10 times [35]. Currently, nickel-based CECs are widely used in industry. Ni-P coatings possess fairly high hardness, corrosion and wear resistance [36,37]. For this reason, a promising direction for the use of chromium-based CECs with DND and nickel-based CECs with DND, when certain conditions are met, is the coating of Ni as a matrix with DND, which does not provide the high strength characteristic for tool strengthening [38,39].

Studies in the field of preparation of multilayer coatings by the combination of electrodeposition and Arc-PVD methods have shown [40,41] that these films have good physical and mechanical properties, and that the incorporation of DND into the coatings further improves their characteristics. The treatment of cemented carbide knives with WC–4 wt.% Co by the combined electrodeposition and Arc-PVD method has been shown to increase the durability period of ZrN-Ni-Co coated cutting tools for laminated chipboard milling. The microhardness of the combined ZrC/Ni-nanodiamonds coatings was 25 $\pm$ 6 GPA. Pilot tests on ZrC/Ni-nanodiamonds coated cutting tools have shown that when milling laminated chipboard, their durability period increases by 1.5 to 1.6 times compared to bare tools.

However, the effects of the combined method of electrodeposition and Arc-PVD treatment on the microstructure, phase composition and tribological effects of the knife blades of milling tools used in wood processing have been little studied. This work is part of the research on combined multilayer systems consisting of nanodiamonds and coatings produced by the Arc-PVD method for modified tool applications, where nanodiamonds are used as a component to extend the tool life.

Therefore, the aim of this research is to describe the preparation of a combined Cr-DND/MoN multilayer coating on WC-Co cemented carbide knives of wood cutting tools using Arc-PVD and electrodeposition methods and the study of their phase composition, microstructure and mechanical properties in terms of hardness and adhesion.

2. Materials and Methods

The substrate was a WC-Co cemented carbide knife purchased from the company Leitz (Germany). The nanodiamonds used in this work (registered trademark "UDA-SP") were produced by JSC "Sinta" (Minsk). The Cr-DND film was deposited from the aqueous chromium electrolyte at a current density of 50 A/dm^2 at 50–60 °C. The electrolyte contained CrO_3 (250 g/dm^3), H_2SO_4 (2.5 g/dm^3) and DND (2–5 g/dm^3 in suspension). The electrodeposition was carried out under magnetic stirring, to homogenize the nanodiamond suspension in the electrolyte. The surface treatment of the carbide knife was carried out thoroughly before electroplating. The detailed preparation process was described previously [42].

The MoN film and the Cu film of the Cr-DND/MoN coating were formed by following the standard steps of the Arc-PVD method under nitrogen atmosphere using the Bulat unit. After being pumped to the base pressure of 10^{-3} Pa, the samples were cleaned with Mo ions and heated to 600–650 °C. The unit had a negative bias voltage of −1 kV. Arc deposition of the MoN coating was performed under the following conditions: arc discharge current of 200 A, substrate bias of −120 V and N_2 pressure of 10^{-1} Pa. The Cu coating was deposited under an arc discharge current of 80 A and the same other conditions as the MoN.

The surface morphology and chemical composition of the cross-section were studied by Hitachi S-4800 scanning electron microscopy (SEM) and energy dispersive X-ray spectroscopy (EDS), respectively.

Structure and phase analysis was performed using an Ultima IV X-ray diffractometer in Cu-K_α radiation in the XRD mode at the scanning speed of 1°/min.

The RS spectra were recorded using a LOTIS TII micro-Raman spectrometer. The excitation was carried out using a solid-state laser with a wavelength of 532 nm, and the laser scan was performed over a film area of 0.8 μm^2.

The hardness of the surface layers was measured by microindentation on an AFFRI-DM8 apparatus using a Vickers diamond pyramid under a load of 0.5–1.0 N with an accuracy of ±15 HV.

The adhesion of the Cr-DND/MoN coating to the substrate was analyzed with a scratch tester. The diamond stylus with a tip diameter of 0.4×10^{-3} m was pulled on the coating with a sliding speed of 0.83×10^{-4} m/s during the increasing load from 0 to 150 N. The loading speed of the indenter was 42 N/s. The ramp load applied was 16 N at the end of the scratch testing. The field of the scratch track and the detection of the fracture mechanism of the coating were studied using optical and scanning electron microscopes (Hitachi S-4800).

3. Results and Discussion

3.1. Microstructural Analysis

The microstructure across the thickness section of the Cr-DND/MoN coating is shown in Figure 1. The samples show a clearly identifiable multilayer structure. It can be seen that the 655 nm thick Cr-DND layer (top of the picture) was much thinner than the lower MoN layer (2.43 μm). There is a 357 nm thick intermediate copper layer between the Cr-DND and MoN layers.

The presence of a copper layer is explained by the deposition technology of CEC Cr-DND, which requires conductive bases to produce a metal-diamond CEC with high adhesion. The MoN coating on which the Cr-DND CEC was deposited was a ceramic characterized by low electrical conductivity. Therefore, a high-electrical-conductivity copper layer was additionally deposited on the MoN layer by the Arc-PVD process, thereby increasing the electrical conductivity of the base on which the Cr-DND CEC was deposited. As a result, the thickness of the Cr-DND/MoN coating reached 3.44 μm.

Figure 1 reveals the dense structure of the MoN layer with columnar growth characteristics. This structure is characteristic of Arc-PVD coatings [43,44].

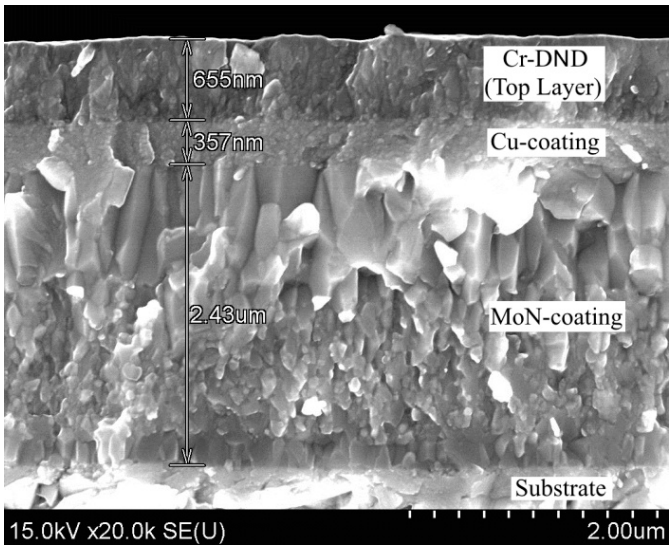

Figure 1. SEM image of the cross-section of the Cr-DND/MoN coating.

In Figure 2, the microstructure of the top layer of the Cr-DND/MoN coating shows an irregular distribution of chromium and carbon in the Cr-DND compound. Figure 2b,c,f shows that in the Cr-DND layer of the combined Cr-DND/MoN coating there was an increase in surface carbon content. This result coincides well with reports that nanodiamonds penetrate a metal plating film as particles trapped within the coating [45] and in most cases form agglomerates [46]. It was proved that carbon is located on the surfaces of Ni-DND/ZrC coatings as nanodiamonds, forming agglomerates 0.7 to 3.5 μm in size [47]. Therefore, the increase in surface carbon content in the Cr-DND layer of the Cr-DND/MoN coating can be explained by the presence of carbon moving to the surface in the form of the nanodiamond agglomerates of the Cr-DND coating during the electrodeposition process of the coating.

The EDS spectrum corresponding to the cross-section of the Cr-DND/MoN coating (Figure 2) shows that the coating had a multilayer structure. The MoN coating was mixed with neither the top Cr-DND film, nor the Cu layer, nor the substrate.

Electrochemical Cr coatings are characterized by the phenomenon of surface self-passivation [48], which is illustrated in Figure 2c,e, showing a high oxygen content in the surface layer of Cr-DND/MoN coating.

Figure 3a,b shows SEM images of the cross-section along the thickness of the sample and the substrate at high resolution. It should be noted that the film was formed of distinct multilayers and that the one in contact with the substrate was characterized by a faceted grain crystal structure (Figure 3b). Figure 3c represents the EDS spectrum of the substrate, and the inset table, its elemental composition. From the EDS results, it can be concluded that the substrate consisted of tungsten carbide with a mass fraction of 3% Co (WC–3 wt.% Co), which is in good agreement with the literature [49], according to which the composition of wood-milling knives corresponds to a fine-grained T03SMG hard alloy from the company TIGRA (Germany).

The EDS spectrum of the top layer of the Cr-DND/MoN coating showed that the Cr-DND layer contained 1.3 ± 0.2 wt.% carbon (Table 1).

Table 1. The elemental composition of the Cr-DND/MoN coating top layer.

Element	Cr	C	Cu
Concentration, wt.%	97.6 ± 3.5	1.3 ± 0.2	1.1 ± 0.2
Concentration, at.%	93.73 ± 2.53	5.39 ± 0.81	0.87 ± 0.09

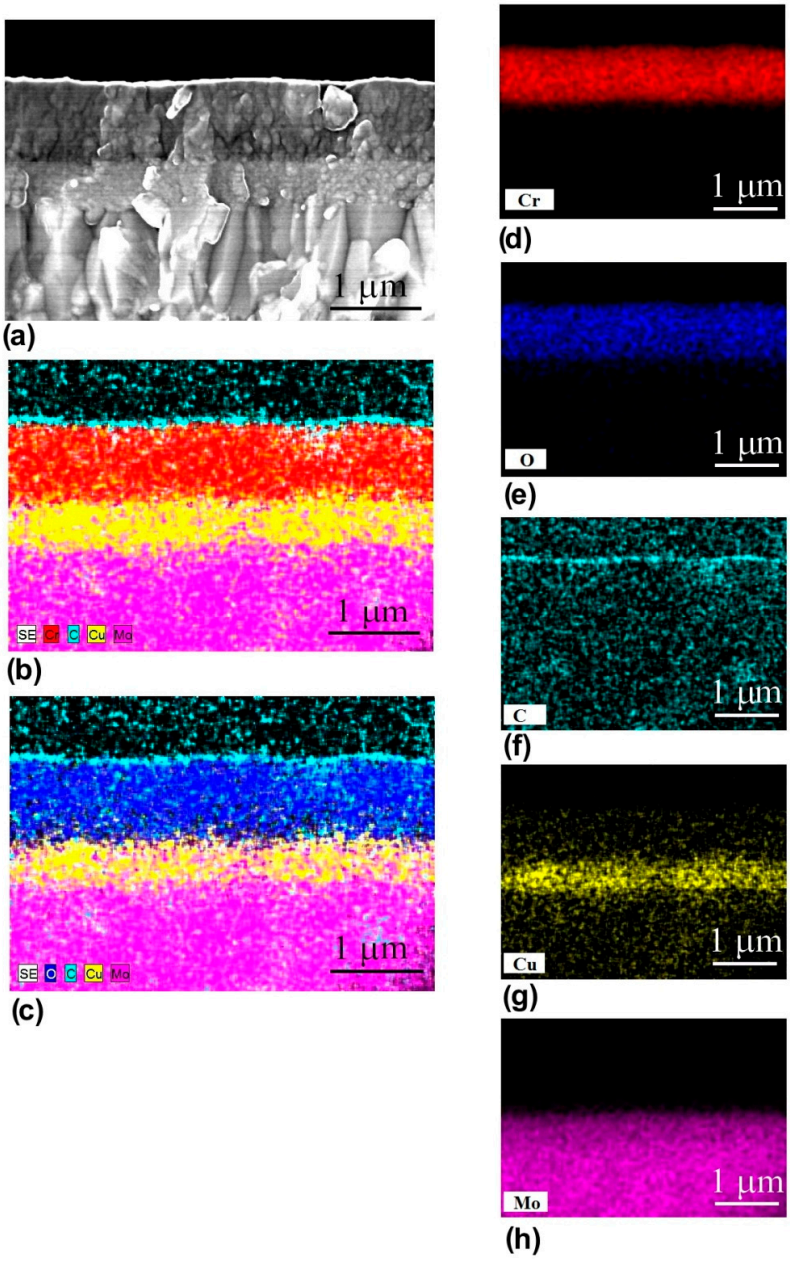

Figure 2. Microstructure of the Cr-DND/MoN coating: (**a**) SEM image and EDS mapping images of the elements (**b**) Cr, C, Cu, Mo; (**c**) O, C, Cu, Mo; (**d**) Cr; (**e**) O; (**f**) C; (**g**) Cu; (**h**) Mo.

3.2. Surface Morphology

The morphology of the MoN films is characterized by an irregular surface typical of coatings deposited by the Arc-PVD method [50]. Figure 4a shows that the surface of the Cr-DND/MoN coating exhibited some roughness, and spheroidal particles with diameters of 1–5 μm could also be observed on the coating surface. Studies of the surface of the Cr-DND/MoN coating at different magnifications (Figure 4b,c) showed that the Cr-DND CEC exhibited a film of aggregates; there was porosity between the aggregates of about 50 nm and within the aggregates of about 10 nm, which is in good agreement with the literature results for the same type of coating [51]. According to this literature, dispersed particle inclusions and nanodiamond aggregates with an average radius of 4.53 μm were found in chrome electrolytes.

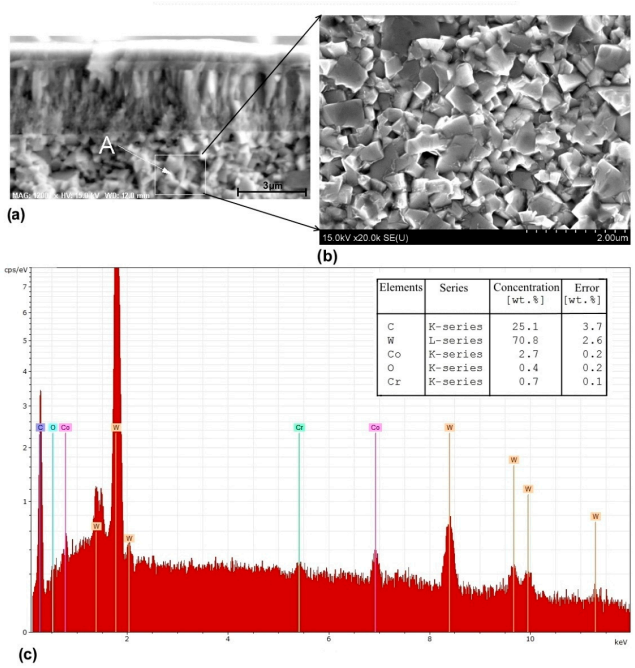

Figure 3. Microstructure and composition of the coated Cr-DND/MoN hard alloy knife: (**a**) SEM cross-section image of Cr-DND/MoN coating; (**b**) SEM high magnification image of indicated zone; (**c**) EDS spectrum, and the table is the elemental analysis of the substrate.

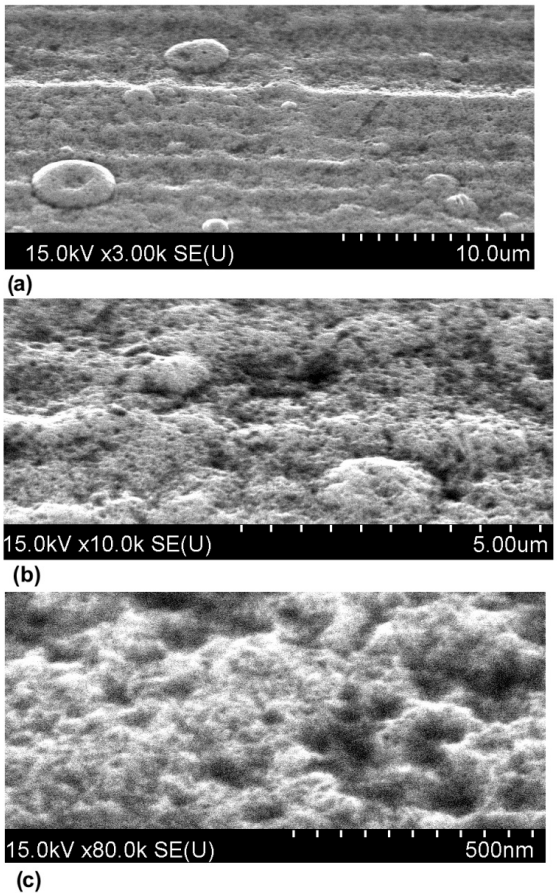

Figure 4. SEM images of the Cr-DND/MoN coating surface at various magnifications: (**a**) 3000×; (**b**) 10,000×; (**c**) 80,000×.

Clearly visible peaks of the X-ray radiation carbon characteristic corresponding to the positions of spheroids (Figure 5) indicate the presence of some compounds containing carbon. Cr-characteristic X-ray radiation had the highest intensity and was evenly distributed throughout the considered area of the surface (Figure 5b). As a result, it can be claimed that the spheroids were compounds containing carbon and chromium.

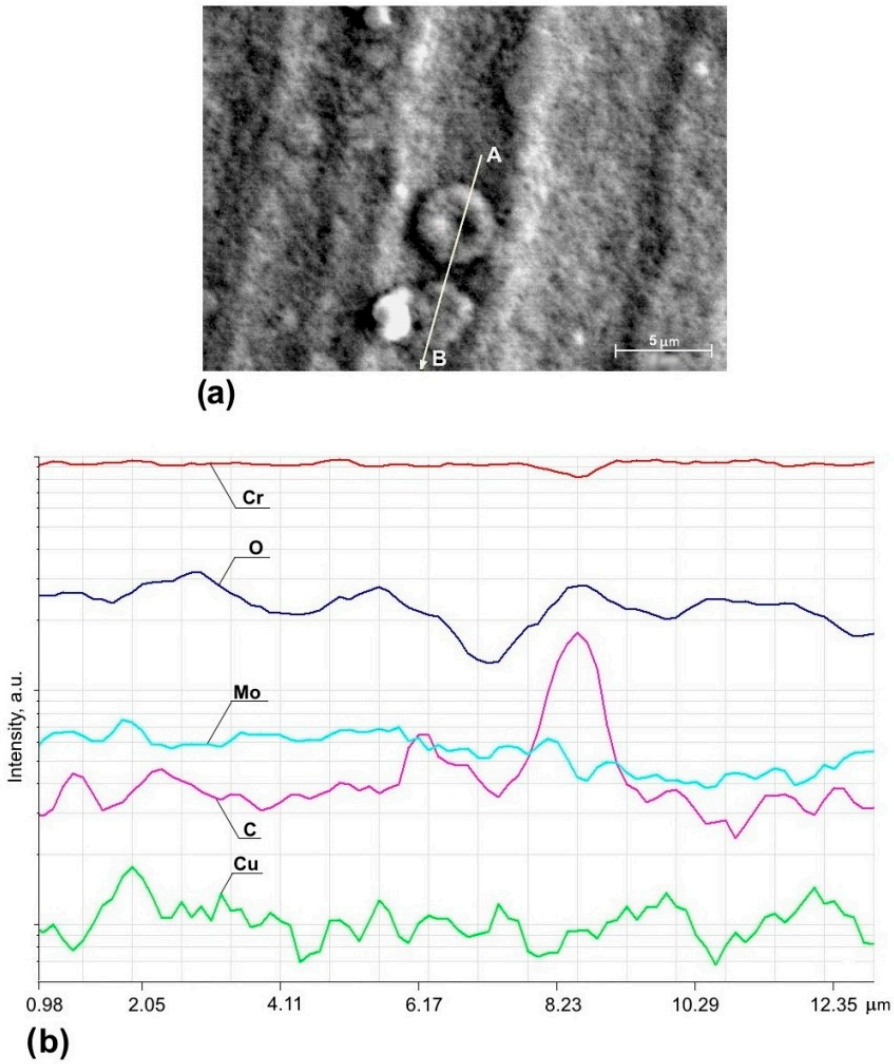

Figure 5. Cr-DND/MoN coated surface: (**a**) SEM image; (**b**) surface distribution of chemical elements (Cr, O, Mo, C, Cu) along the AB line scanning, achieved by X-ray radiation experiments.

Nanodiamond particles tend to form agglomerates, as reported by various authors [39,41,52]. Hence, the spheroids were aggregates of nanodiamonds at the top of the Cr-DND layer in the coating.

3.3. Phase Analysis

The XRD pattern of the Cr-DND/MoN coating is shown in Figure 6, and it does not reveal any crystalline phase. The XRD studies of the MoN layer of the Cr-DND/MoN coating were carried out considering the results obtained previously when searching for the formation of two different MoN phases (β-Mo_2N and cubic γ-Mo_2N) as a function of nitrogen pressure, displacement stress and substrate temperature during Arc-PVD deposition [53,54].

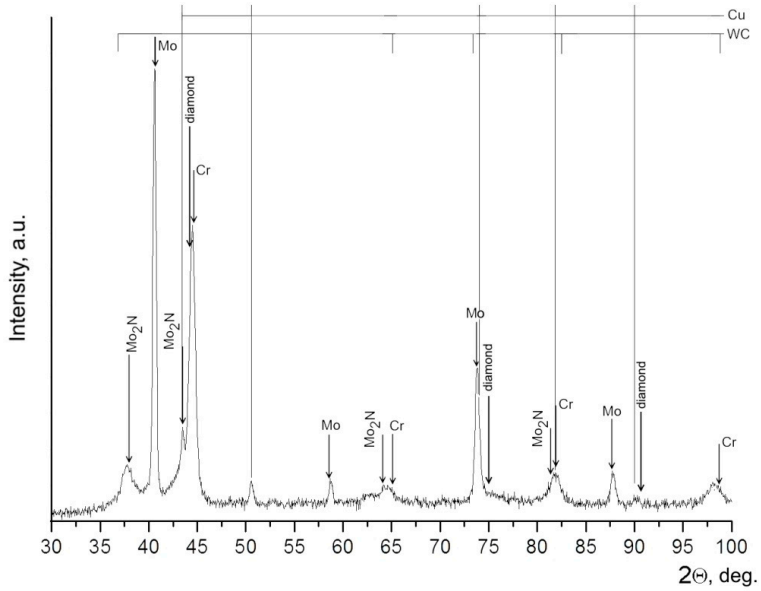

Figure 6. XRD pattern corresponding to the prepared Cr-DND/MoN coating.

Analysis of the XRD pattern corresponding to the Cr-DND/MoN coating revealed the existence of a γ-Mo_2N phase with a B1 structure (fcc, NaCl). The observed XRD peaks of molybdenum and cuprum belong to the α-Mo and α-Cu phases with an fcc lattice.

The formation of the α-Mo phase can be explained by the dependence of the coating's nitrogen content on nitrogen pressure. It has been shown that in coatings formed at pressure 9.33×10^{-2} Pa, the nitrogen content is nearly two times lower than in coatings produced at a higher pressure, 0.4 Pa [55].

It can be observed that there is an intense (111) crystallographic plane peak of diamond located at 43.9°, which overlaps with the intense Cr peak corresponding to the (111) crystallographic plane diffraction. From these results, it can be deduced that the coating consisted of a Cr-DND phase with (111) crystallographic plane dominance. Other diamond XRD peaks corresponding to the (220) and (311) crystallographic planes were observed at 2θ ~ 75.3° and 91.5°, respectively. Furthermore, reflections corresponding to the (111), (220) and (311) crystallographic planes are attributed to the diamond-like lattice with a parameter $a_0 = 3.568 \pm 0.008$ Å [26,56].

As the peaks corresponding to the γ-Mo_2N, α-Mo, α-Cu, Cr and Cr-DND phases are clearly visible in the XRD diffractogram, it proves that there was no solid solubility. In addition, he low intensity peaks of the tungsten carbide substrate were observed for the Cr-DND/MoN coating. These results highlight the presence of γ-Mo_2N, α-Mo, α-Cu, Cr and Cr-DND phases and nanodiamonds in the Cr-DND/MoN coating.

3.4. Raman Spectra

The Raman imaging was performed to see the distinct phases in the carbon material of the prepared coating. Figure 7 shows the Raman spectra for the initial DND sample and the Cr-DND/MoN coated sample.

For the original DND sample, the Raman spectrum can be represented as a superposition of three peaks with maxima located at 1322, 1570 and 1625 cm^{-1}. Analysis of the spectra showed a shift of the peak maximum from that of the sp^3-carbon at 1332 cm^{-1}, which is characteristic of large diamond crystals. A broadening of this peak was also found (Figure 7) and is associated with the small crystallite size in DND. Figure 7 also shows that in the background of the peak at 1322 cm^{-1} there is a peak with a characteristic frequency shift at 1350 cm^{-1} belonging to the D-band with sp^2-hybrid bonds [56].

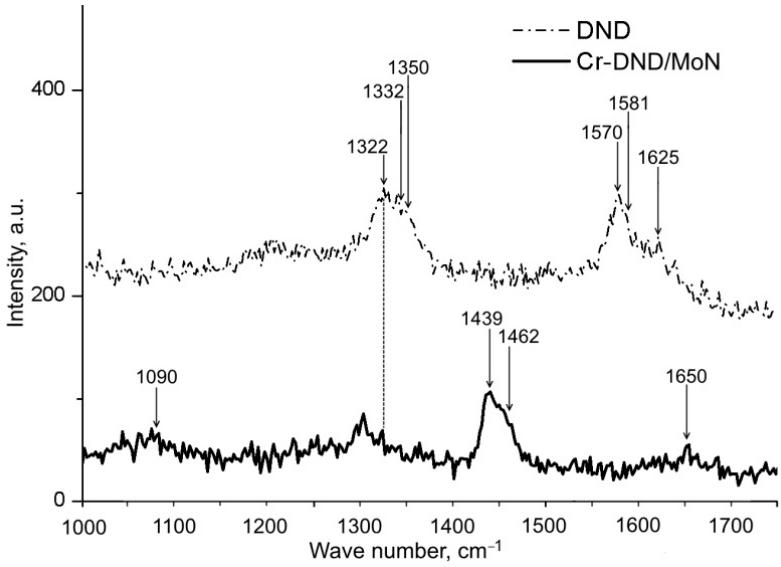

Figure 7. Raman spectra of DND sample and the Cr-DND/MoN coated sample.

The second peak at 1570 cm^{-1} belongs to the G-band, which is usually positioned 1581 cm^{-1} for the DND sample. The D and G peaks at 1350 and 1581 cm^{-1}, respectively, are related to the known A_{1g} and E_{2g} modes of the sp^2-hybrid bond carbon atom vibrations [57]. In addition to the aforementioned peak located at 1570 cm^{-1}, depending on the parameters of the DND synthesis process, there is another peak located at 1625 cm^{-1} in the region 1600–1640 cm^{-1}, which relates to the carbon of the sp^2-hybrid bonds [56].

The Raman spectrum of the Cr-DND/MoN coated sample showed a relatively weak C-O stretching band at 1090 cm^{-1} and enhanced C-H bending plane vibration at 1439–1462 cm^{-1}. This indicates the existence of a carbonyl group and a hydrocarbon group on the DND surface, as reported by other authors [58]. The second peak at 1300 cm^{-1} corresponds to the displacement of the sp^3-hybridized carbon peak (the diamond phase) at 1322 cm^{-1} and can be attributed to the size effect [59]. Furthermore, a peak at 1650 cm^{-1}, which appeared in the Raman spectrum of the Cr-DND/MoN coated sample, is related to the presence of sp^2-hybridized carbon.

Therefore, the Raman spectrum of the Cr-DND/MoN coated sample proved the presence of DND with small diamond crystallites and nanodiamonds on the surface with functional groups.

3.5. Microindentation

For the Cr-DND/MoN coating, the maximum microhardness of 14 ± 1 GPa was observed for a load of 200 g (the average penetration depth of the diamond indenter was ~2.4 μm), and a microhardness of 12 ± 1 GPa was observed for a load of 100 g (the indenter penetration was ~1.7 μm). The almost identical microhardness values of the Cr-DND/MoN coating can be explained by the penetration of the indenter to the hard MoN layer, as the thickness of the top layers deposited on the MoN layer shown in Figure 1, was on average ~1.0 μm. The studies carried out proved that the synthesized coatings of γ-Mo_2N at a nitrogen pressure of 0.4 Pa on HSS substrates had a hardness of 3372 ± 100 kg/mm^2 [53]. When obtaining the CrN and γ-Mo_2N phases of the MoN/CrN coating with a cubic lattice, a maximum hardness of 35.5 GPa was observed [22].

The maximum microhardness of 16.2 ± 1.8 GPa at a load of 100 g (average penetration depth of the indenter—about 1.5 μm) was observed for the Cr-DND coating deposited on a hard alloy substrate (WC–3 wt.% Co) of knife mills from the Leitz company, having the microhardness of 21 ± 2 GPa [40].

The work of Vinokurov [52] investigated the physico-mechanical properties of chromium-nanodiamond CECs (NDs) deposited from Cr(III)-based electrolytes, and it was shown

that the microhardness of the coatings increases from 710 ± 41 HV (pure chromium) to 954 ± 40 HV (CECs) with the introduction of nanodiamond particles into the chromium electrolyte at a concentration of 20 g/L. Furthermore, it was shown that the optimum amount of nanodiamonds in the Cr-DND CECs, at which a maximum of microhardness of the precipitates was observed, is 5.6 wt.%. Moreover, it was also shown that the optimal amount of nanodiamonds in the Cr-DND CEC, at which a maximum of microhardness of the precipitates was observed, is 5.6 wt.%. In this case, the optimal concentration of nanodiamond particles in Cr(III)-based electrolytes is 17 g/L.

The EDS spectrum of the surface of the Cr-DND/MoN coating showed that the Cr-DND top layer, which was formed using a nanodiamond solution with a concentration of 2–5 g/L, consisted of 1.3 ± 0.2 wt.% carbon (Table 1).

From the results discussed above, the microhardness of the Cr-DND/MoN coating increases with the amount of nanodiamonds in the coating.

3.6. Scratch Test Results

The adhesion properties of the coating are related to all the interatomic interactions at the interface between the coating and the substrate materials, including the elastic properties of the coating and the substrate, the fracture strength, the distribution of pores and other defects in the material, the loading conditions and the frictional behavior [60]. It is known that the adhesion strength is defined as a measure of the coating's resistance to fracture and can be determined by measuring the critical load L_c.

Using a progressive load for the Cr-DND/MoN coating, we found that the critical load L_c was about 93 ± 1 N (Figure 8). Furthermore, analysis of the load curve (Figure 8) and scratch traces (Figures 8 and 9) revealed several stages of coating destruction. Figure 8 shows that initially, monotonous penetration of the indenter into the coating occurred, and as the load increased considerably over the short length of the trace, the coating exhibited strong resistance to the penetration of the indenter. In addition, there was an almost monotonic dependence of the load value on the short trace length. From the optical images of the scratch paths (Figure 8), it can be proposed that the main failure modes of the adhesive are cohesive failure.

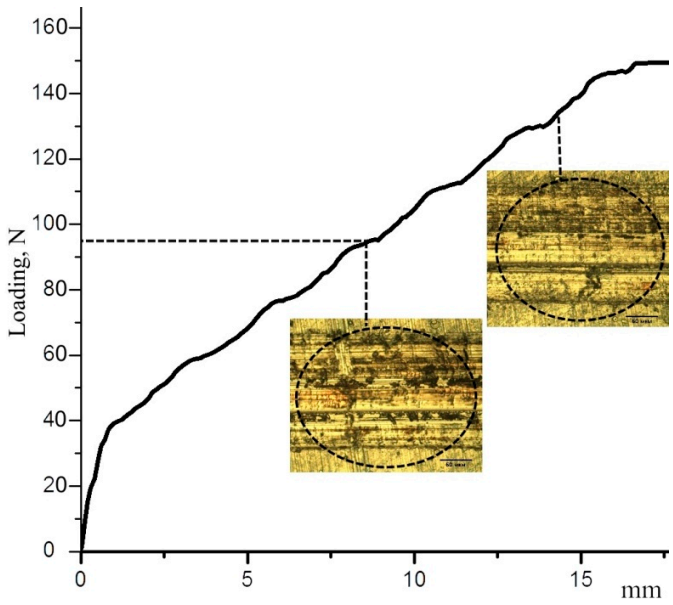

Figure 8. The graph of the loading curve. The inserts are optical images of the striped region of the Cr-DND/MoN coating.

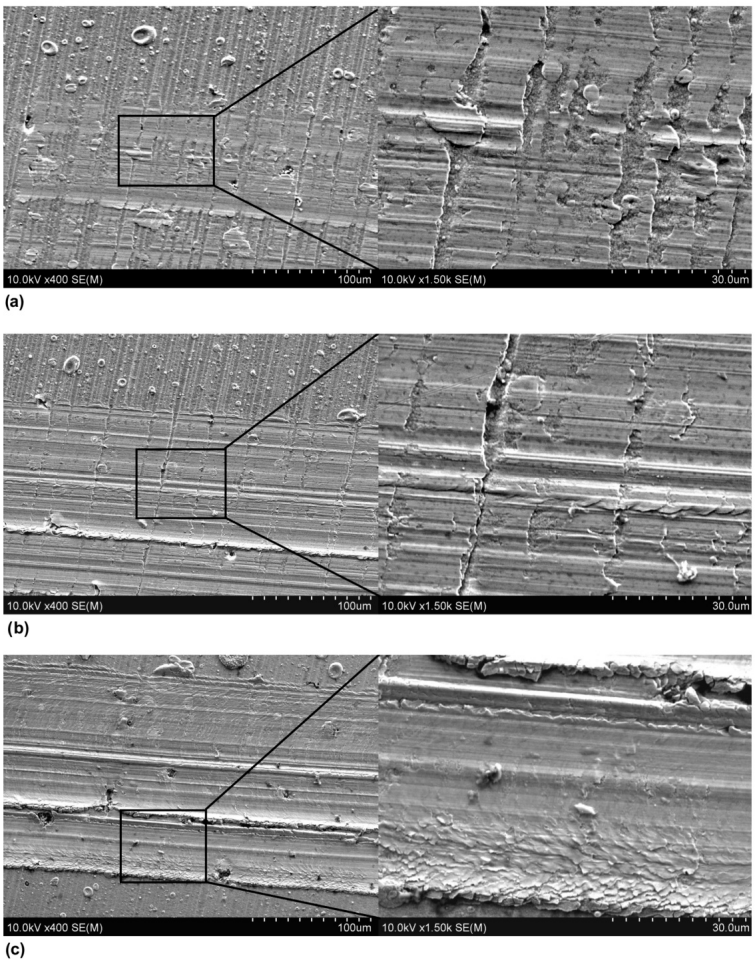

Figure 9. SEM images of the scratch trace on the Cr-DND/MoN coating: (**a**) at the beginning of the path; (**b**) in the middle of the path; (**c**) at the end of the path.

To further investigate the worn surface of the scratch pattern, SEM observation of the worn surface of the coating was performed. The content of characteristic elements in the worn surface was analyzed by EDX.

Figures 9–11 show the surfaces of the wear tracks on the coating and the corresponding EDX mapping images. As it can be seen in these images, the tested coating exhibited adhesive wear caused by the transfer of material from one contact surface to the other and showed uniform wear of the coating with the profile wear track of symmetrical shape and similar shape of the counter body (Figure 9a–c, magnification 400×). There was no coating delamination or flaking around the scratch line. The width and shape of the break line in the coating were fairly uniform. At the beginning and middle of the track (Figure 9a,b), under a normal load of 5–20 N, cracks propagating perpendicular to the scratch channel were found inside the scratch channel. A worn surface was taken from a shallow groove inside the scratch channel. The formation of cracks inside the scratch channel indicates brittle damage to the coating and substrate duo under the progressive load of the diamond stylus. The middle and the end of the tracks showed areas of worn surfaces (Figure 9b,c), which can be attributed to surface grooves and brittle fracture of the protuberances. The surface furrows are the response to the deformation caused by the penetration of the indenter tip and its movement over the surface. It can be seen in Figure 9 that the width of the wear track increased during the scratching process. Scattered wear debris (white particles) was observed on and next to the wear track (Figure 9c (magnification 1500×)). Studies of the wear behavior of the (Ti, Mo)N film [61] and the TiCN film [62] showed that the wear debris accumulated in the scratch path area. The wear debris of the (Ti, Mo)N film was

mainly composed of Mo and Ti oxides or Fe oxide from the counter body. An increase in the oxygen content in the finish track of the Cr-DND/MoN coating (Table 2) could be seen compared to the initial EDX analysis of the coating (Table 1).

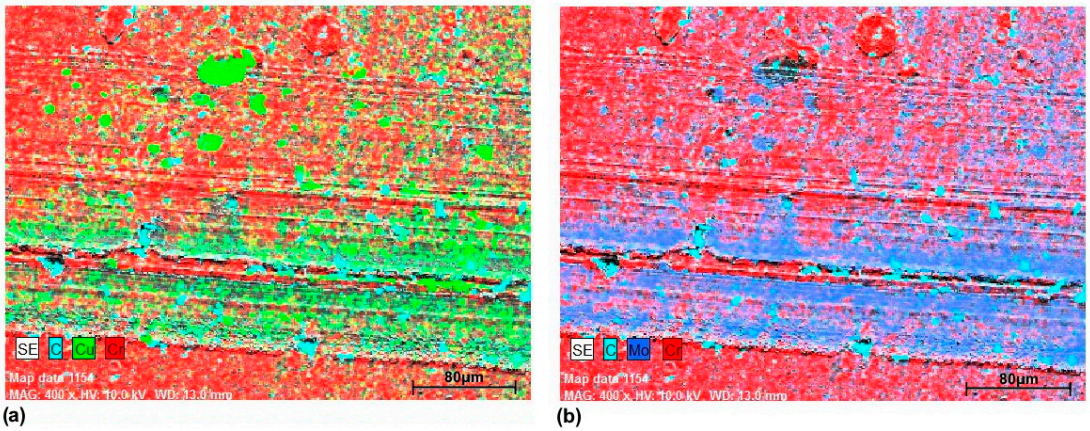

Figure 10. EDX mapping images of different chemical elements forming the prepared Cr-DND/MoN coating: (**a**) C, Cu, Cr; (**b**) C, Mo, Cr—taken from Figure 9c (magnification 400×).

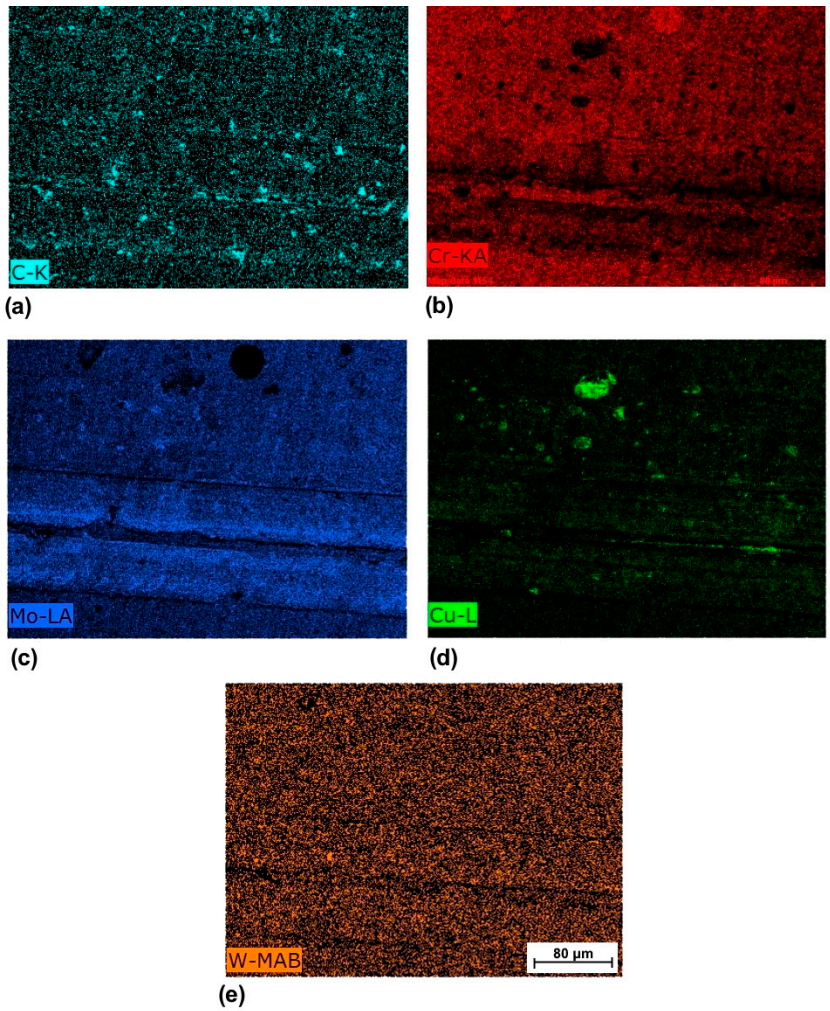

Figure 11. EDX mapping images of (**a**) C, (**b**) Cr, (**c**) Mo, (**d**) Cu and (**e**) W in the Cr-DND/MoN coating presented in Figure 9c (magnification 400×).

Table 2. The elemental composition at the end of the scratch track of the Cr-DND/MoN coating.

Element	Cr	C	Mo	O	N	Cu	W
Concentration, wt.%	39.9 ± 1.6	5.2 ± 0.7	38.8 ± 1.5	5.9 ± 0.8	2.5 ± 0.4	7.6 ± 1.0	0.1 ± 0.0
Concentration, at.%	33.85 ± 0.91	19.08 ± 2.86	17.80 ± 0.23	16.29 ± 2.40	7.64 ± 1.13	5.30 ± 0.53	0.02 ± 0.00

From this result, we can conclude that the wear debris in the scratch track of the coating Cr-DND/MoN consisted of Cr, Cu and Mo oxides.

Figure 10 shows EDX mapping images of the elements C, Cu, Mo and Cr in the Cr-DND/MoN coating shown in Figure 9c (magnification 400×).

Figure 11a–e reveals EDX mapping image data of the elements (a) C, (b) Cr, (c) Mo, (d) Cu and (e) W in the Cr-DND/MoN coating shown in Figure 9c (magnification 400×).

It can be seen that the top Cr-DND layer of the Cr-DND/MoN coating in the scratch channel was considerably destroyed but did not disappear, and the bottom MoN layer on the substrate was slightly worn away in the Cr-DND/MoN coating presented in Figure 9c (magnification 400×). It can also be concluded that the penetration depth of the indentor into the Cr-DND/MoN coating was 1.1–1.6 μm at the end of the scratch track.

The results obtained show that the wear of the scratched Cr-DND/MoN coating does not lead to its crumbling, but rather to its fracture by the cohesion mechanism. Furthermore, an analysis of the critical load L_c value and the scratch trace revealed good adhesion strength of the Cr-DND/MoN coating, higher than the results reported in the literature for coatings deposited on the WC-Co substrate [44,63].

Figures 10 and 11 also show the presence of spheroidal particles consisting of chromium and carbon on the surfaces of Cr-DND/MoN coatings, as shown in Figure 5.

4. Conclusions

The combined Cr-DND/MoN coating was prepared by Arc-PVD and electroplating methods on the wood-cutting knife edges of a mill. It was shown that the Cr-DND/MoN coating consisted of distinguished layers of Cr-DND (top), Cu (middle) and MoN (bottom). The thicknesses were measured to be 2.43, 357 and 655 nm for the MoN, Cu and Cr-DND layers, respectively. Furthermore, the Cr-DND/MoN coating was characterized by distinct phases: γ-Mo_2N phase; α-Mo, α-Cu, Cr and Cr-DND phase; and nanodiamonds.

The MoN layer was found to be a dense structure with columnar growth characteristics. The observed structure is characteristic of Arc-PVD deposited coatings. In addition, an increase in the carbon content of the surface of the Cr-DND layer was observed due to the displacement of non-built nanodiamond agglomerates in the structure of the Cr-DND layer towards the surface of the coating during its electrodeposition process. The substrate structure was a crystalline cemented tungsten carbide (WC–3 wt.% Co). The Cr-DND CEC top layer of the Cr-DND/MoN coating was characterized by inclusion of spheroidal particles ranging from 1 to 5 μm in diameter that were fairly well dispersed and had some porosity. The spheroids were formed by agglomerates of nanodiamonds in the Cr-DND layer of the combined coating.

The microhardness of the Cr-DND/MoN coating was shown to increase with the concentration of nanodiamonds incorporated in the CEC chromium layer. The upper microhardness of about 14 ± 1 GPa was measured for the Cr-DND/MoN coating, without evaluating the maximum microhardness.

The critical load of the Cr-DND/MoN coating was estimated to be approximately 93 ± 1 N. In addition, the results of the scratch tests showed that the layers of the Cr-DND/MoN coating fractured by the cohesive mechanism. Furthermore, there was no absolute failure of the coating adhesion due to spalling damage. Furthermore, the critical load value and the scratch track revealed a rather high value for the adhesion strength of the Cr-DND/MoN coating with a WC-Co base.

Author Contributions: Conceptualization, V.C.; methodology, V.C., V.Z. and A.K.; validation, V.C.; investigation, V.C., V.Z. and A.K.; resources, V.C., A.K. and R.S.; formal analysis, V.C., V.Z. and A.T.; data curation, V.C., V.Z. and A.T.; writing—original draft preparation, V.C.; writing—review and editing, V.C. and A.T.; supervision, A.T.; project administration, V.C.; funding acquisition, V.C. All authors have read and agreed to the published version of the manuscript.

Funding: This research was financed by the State Budget Program of Science Researches of the Republic of Belarus (task No. 8.3, "Technologies of processing and creation of materials by electromagnetism, plasma-beam and foundry-deformation"; assignment No. 3.2.7).

Institutional Review Board Statement: Not applicable.

Informed Consent Statement: Not applicable.

Data Availability Statement: Data available on request due to restrictions privacy or ethical.

Acknowledgments: The authors would like to express their gratitude to the State Centre "Belmikroanaliz" of the holding company "INTEGRAL" for providing the necessary facilities for carrying out these studies.

Conflicts of Interest: The authors declare no conflict of interest.

References

1. Catalogue Kanefusa Woodworking. Available online: https://kanefusa-shop.ru/manuals/ (accessed on 1 October 2015).
2. LEKSIKON Leitz. *Leitz Co. Catalog, on CD-ROM*; Leitts Instrumenty: Moscow, Russia, 2011. (In Russian)
3. Catalogues Sandvik Coromant. Available online: http://sandvik-coromant.ru/catalogues/ (accessed on 3 May 2016).
4. Catalogs ISCAR Ltd. Manufacturer of Metalworking Tools. Available online: https://www.iscar.com/newarticles.aspx/countryid/1/newarticleid/2393/ (accessed on 13 June 2018).
5. Egashira, K.; Hosono, S.; Takemoto, S.; Masao, Y. Fabrication and cutting performance of cemented tungsten carbide micro-cutting tools. *Precis. Eng.* **2011**, *35*, 547–553. [CrossRef]
6. García, J.; Ciprés, V.; Blomqvist, A.; Kaplan, B. Cemented carbide microstructures: A review. *Int. J. Refract. Met. Hard Mater.* **2019**, *80*, 40–68. [CrossRef]
7. Guo, X.; Ekevad, M.; Grönlund, A.; Marklund, B.; Cao, P. Tool Wear and Machined Surface Roughness during Wood Flour/Polyethylene Composite Peripheral Up-milling using Cemented Tungsten Carbide Tools. *BioResources* **2014**, *9*, 3779–3791. [CrossRef]
8. Abrazumov, V.V. Wear Resistance of Cutting Tools during Machining of Wooden Composite Materials. Doctoral Thesis, State Forest University, Moscow, Russia, 2009. (In Russian)
9. Darmawan, W.; Rahayu, I.; Nandika, D.; Marchal, R. The importance of extractives and abrasives in wood materials on the wearing of cutting tools. *BioResources* **2012**, *7*, 4715–4729. [CrossRef]
10. Sommer, F.; Kern, F.; Gadow, R. Injection molding of ceramic cutting tools for wood-based materials. *J. Eur. Ceram. Soc.* **2013**, *33*, 3115–3122. [CrossRef]
11. Zhu, Z.; Guo, X.; Ekevad, M.; Cao, P.; Na, B.; Zhu, N. The effects of cutting parameters and tool geometry on cutting forces and tool wear in milling high-density fiberboard with ceramic cutting tools. *Int. J. Adv. Manuf. Technol.* **2017**, *91*, 4033–4041. [CrossRef]
12. Gilewicz, A.; Warcholinski, B.; Myslinski, P.; Szymanski, W. Anti-wear multilayer coatings based on chromium nitride for wood machining tools. *Wear* **2010**, *270*, 32–38. [CrossRef]
13. Grigoriev, S.N.; Vereschaka, A.A.; Fyodorov, S.V.; Sitnikov, N.N.; Batako, A.D. Comparative analysis of cutting properties and nature of wear of carbide cutting tools with multi-layered nano-structured and gradient coatings produced by using of various deposition methods. *Int. J. Adv. Manuf. Technol.* **2017**, *90*, 3421–3435. [CrossRef]
14. Kathrein, M.; Michotte, C.; Penoy, M.; Polcik, P.; Mitterer, C. Multifunctional multi-component PVD coatings for cutting tools. *Surf. Coat. Technol.* **2005**, *200*, 1867–1871. [CrossRef]
15. Kuleshov, A.K.; Uglov, V.V.; Rusalsky, D.P.; Grishkevich, A.A.; Chaevski, V.V.; Haranin, V.N. Effect of ZrN and Mo–N Coatings and Sulfacyanization on Wear of Wood-Cutting Knives. *J. Frict. Wear* **2014**, *35*, 201–209. [CrossRef]
16. Pshyk, A.V.; Kravchenko, Y.; Coy, E.; Kempiński, M.; Iatsunskyi, I.; Załęski, K.; Pogrebnjak, A.D.; Jurga, S. Microstructure, phase composition and mechanical properties of novel nanocomposite (TiAlSiY)N and nanoscale (TiAlSiY)N/MoN multifunctional heterostructures. *Surf. Coat. Technol.* **2018**, *350*, 376–390. [CrossRef]
17. Gilewicz, A.; Warcholinski, B.; Szymanski, W.; Grimm, W. CrCN/CrN+ta-C multilayer coating for applications in wood processing. *Tribol. Int.* **2013**, *57*, 1–7. [CrossRef]
18. Wang, M.; Miyake, S. Surface Morphology and Tribological Properties of Nanoscale (Ti, Al, Si, C)N Multilayer Coatings Deposited by Reactive Magnetron Sputtering. In *Tribology, Lubricants and Additives*; Johnson, D.W., Ed.; IntechOpen Ltd: London, UK, 2018; pp. 77–100.
19. Zhang, Y.; Yu, L.; Fu, T.; Wang, J.; Shen, F.; Cui, K. Microstructure evolution and growth mechanism of Si-MoSi2 composite coatings on TZM (Mo-0.5Ti-0.1Zr-0.02 C) alloy. *J. Alloy Compd.* **2022**, *894*, 162403. [CrossRef]

20. Zhang, Y.; Yu, L.; Fu, T.; Wang, J.; Shen, F.; Cui, K.; Wang, H. Microstructure and oxidation resistance of Si-MoSi2 ceramic coating on TZM (Mo-0.5Ti-0.1Zr-0.02C) alloy at 1500 °C. *Surf. Coat. Technol.* **2022**, *431*, 128037. [CrossRef]
21. Gilewicz, A.; Warcholinski, B. Deposition and characterisation of Mo_2N/CrN multilayer coatings prepared by cathodic arc evaporation. *Surf. Coat. Technol.* **2015**, *279*, 126–133. [CrossRef]
22. Pogrebnyak, A.D.; Bondar, O.V.; Zhollybekov, B.; Konstantinov, S.; Konarski, P.; Beresnev, V.M.; Kupchishin, A.I. Influence of the bilayer thickness of nanostructured multilayer MoN/CrN coating on its microstructure, hardness, and elemental composition. *Phys. Solid State* **2017**, *59*, 1798–1802. [CrossRef]
23. Pogrebnjak, A.D.; Beresnev, V.M.; Bondar, O.V.; Postolnyi, B.O.; Zaleski, K.; Coy, E.; Jurga, S.; Lisovenko, M.O.; Konarski, P.; Rebouta, L.; et al. Superhard CrN/MoN coatings with multilayer architecture. *Mater. Des.* **2018**, *153*, 47–59. [CrossRef]
24. Tseluikin, V.N. Tribological properties of composite electrochemical nickel-based coatings. *J. Frict. Wear* **2010**, *31*, 356–358. [CrossRef]
25. Gomez, H.; Durham, D.; Xiao, X.; Lukitsch, M.; Lu, P.; Chou, K.; Sachdev, A.; Kumar, A. Adhesion analysis and dry machining performance of CVD diamond coatings deposited on surface modified WC–Co turning inserts. *J. Mater. Process. Technol.* **2012**, *212*, 523–533. [CrossRef]
26. Shen, X.; Wang, X.; Sun, F.; Ding, C. Sandblasting pretreatment for deposition of diamond films on WC-Co hard metal substrates. *Diam. Relat. Mater.* **2017**, *73*, 7–14. [CrossRef]
27. Burkat, G.K.; Dolmatov, V.Y. Application of ultrafine-dispersed diamonds in electroplating. *Phys. Solid State* **2004**, *46*, 703–710. [CrossRef]
28. Boudou, J.P.; Curmi, P.A.; Jelezko, F.; Wrachtrup, J.; Aubert, P.; Sennour, M.; Balasubramanian, G.; Reuter, R.; Thoreland, A.; Gaffet, E. High yield fabrication of fluorescent nanodiamonds. *Nanotechnology* **2009**, *20*, 235–602. [CrossRef]
29. Yang, G.W.; Wang, J.B.; Liu, O.X. Preparation of nano-crystalline diamonds using pulsed laser induced reactive quenching. *J. Phys. Condens. Matter* **1998**, *10*, 7923–7927. [CrossRef]
30. Dolmatov, V.Y. Detonation synthesis ultradispersed diamonds: Properties and applications. *Rus. Chem. Rev.* **2001**, *70*, 607–626. [CrossRef]
31. Dolmatov, V.Y. Detonation Nanodiamonds. In *Preparation, Properties, and Applications*; SPO "Professional": St. Petersburg, Russia, 2011. (In Russian)
32. Kononov, A.G.; Sachivko, Y.S.; Korzhenevskiy, A.P.; Shtemplyuk, R.G. Thermal stability of chromium coatings modified with nano-sized oxygen-containing additives. *Mech. Mach. Mech. Mater.* **2015**, *4*, 353–357.
33. Kubrak, P.B.; Drozdovich, V.B.; Zharski, I.M.; Chaevskiy, V.V. Electrodeposition of Composite Coatings Containing Carbon-based Nanomaterials and Properties of Coatings Obtained. *Electroplat. Surf. Treat.* **2012**, *XX*, 43–49.
34. Shenderova, O.; Gruen, D. *Ultrananocrystalline Diamond, Synthesis, Properties, and Application of UNCD*, 2nd ed.; William Andrew Pub.: Kidlington, UK, 2006.
35. Vityaz, P.A.; Zhornik, V.I.; Ilyushchenko, A.F.; Senyut, V.T.; Komarov, A.I.; Korzhenevskiy, A.P.; Ivakhnik, A.V. *Nanodiamonds of Detonation Synthesis: Preparation and Application*; Belaruskaya Navuka: Minsk, Belarus, 2013. (In Russian)
36. Chang, M.K.; Chen, C.H.; Chen, B.H. Fabrication of magnetic nickel-tungsten-phosphorus particles by electroless deposition. *J. Magn. Magn. Mater.* **2006**, *305*, 342–347. [CrossRef]
37. Yan, M.; Ying, H.G.; Ma, T.Y. Improved microhardness and wear resistance of the as-deposited electroless Ni–P coating. *Appl. Surf. Sci.* **2008**, *202*, 5909–5913. [CrossRef]
38. Nenashev, M.V.; Ibatullin, I.D.; Ganigin, S.J.; Galljamov, A.R.; Neyaglova, R.R. Advanced technologies, properties and application of electrochemical nanostructured coverings. *VESTNIK Samara Univ. Aerosp. Mech. Eng.* **2011**, *3-1*, 189–196. (In Russian)
39. Polushin, N.I.; Kudinov, A.V.; Zhuravlev, V.V.; Stepareva, N.N.; Maslov, A.L. Dispersed strengthening of a diamond composite electrochemical coating with nanoparticles. *Russ. J. Non-Ferr. Met.* **2013**, *54*, 412–416. [CrossRef]
40. Chayeuski, V.; Zhylinskiy, V.; Grishkevich, A.; Rudak, P.; Barcik, Š. Influence of high energy treatment on wear of edges knives of wood-cutting tool. *MM Sci. J.* **2016**, *6*, 1519–1523. [CrossRef]
41. Chayeuski, V.; Zhylinski, V.; Cernashejus, O.; Visniakov, N.; Mikalauskas, G. Structural and Mechanical Properties of the ZrC/Ni-Nanodiamond Coating Synthesized by the PVD and Electroplating Processes for the Cutting Knifes. *J. Mat. Eng. Perf.* **2019**, *28*, 1278–1285. [CrossRef]
42. Chayeuski, V.; Zhylinski, V.; Kuleshov, A.; Rudak, P.; Barcík, Š. Wear of the ZrC and ZrC/Ni-ultradisperse diamonds coated edges knives of wood-cutting tool. In *Chip and Chipless Woodworking Processes, Proceedings of 11th International Science Conference, Zvolen, the Slovak Republic, 13–15 September 2018*; The Technical University in Zvolen: Zvolen, Slovakia, 2018; pp. 59–64.
43. Warcholinski, B.; Gilewicz, A.; Kuprin, A.S.; Tolmachova, G.N.; Ovcharenko, V.D.; Kuznetsova, T.A.; Zubar, T.I.; Khudoley, A.L.; Chizhik, S.A. Mechanical properties of Cr-O-N coatings deposited by cathodic arc evaporation. *Vacuum* **2018**, *156*, 97–107. [CrossRef]
44. Sampath Kumar, T.; Balasivanandha Prabu, S.; Manivasagam, G. Metallurgical Characteristics of TiAlN/AlCrN Coating Synthesized by the PVD Process on a Cutting Insert. *J. Mat. Eng. Perf.* **2014**, *23*, 2877–2884. [CrossRef]
45. Malatji, N.; Popoola, P.A.I. Tribological and Corrosion Performance of Electrodeposited Nickel Composite Coatings. In *Electrodeposition of Composite Materials*; Mohamed, A.M.A., Golden, T.D., Eds.; IntechOpen Limited: London, UK, 2016; pp. 205–230.
46. Katzensteiner, A.; Rosalie, J.M.; Pippan, R.; Bachmaier, A. Synthesis of nanodiamond reinforced silver matrix nanocomposites: Microstructure and mechanical properties. *MSEA* **2020**, *782*, 139–254. [CrossRef]

47. Chayeuski, V.V.; Zhylinski, V.V.; Rudak, P.V.; Rusalsky, D.P.; Višniakov, N.; Cernašejus, O. Characteristics of ZrC/Ni-UDD coatings for a tungsten carbide cutting tool. *Appl. Surf. Sci.* **2018**, *446*, 18–26. [CrossRef]
48. Danilov, F.I.; Protsenko, V.S.; Butyrina, T.E.; Krasinskii, V.A.; Baskevich, A.S.; Kwon, S.C.; Lee, J.Y. Electrodeposition of nanocrystalline chromium coatings from Cr(III)-based electrolyte using pulsed current. *Prot. Met. Phys. Chem. Surf.* **2011**, *47*, 598–605. [CrossRef]
49. Alifanov, A.V.; Grishkevich, A.A.; Chayevskii, V.V.; Garanin, V.N. Influence of TiN-coatings hard alloy knives on exploitation of wood-cutting milling tool when processing laminated chipboard. *Proc. BSTU* **2012**, *2*, 146–149.
50. Paiva, J.M.; Fox-Rabinovich, G.; Junior, E.L.; Stolf, P.; Ahmed, Y.S.; Martins, M.M.; Bork, C.; Veldhuis, S. Tribological and Wear Performance of Nanocomposite PVD Hard Coatings Deposited on Aluminum Die Casting Tool. *Materials* **2018**, *11*, 358. [CrossRef]
51. Tseluikin, V.N. On the Structure and Properties of Composite Electrochemical Coatings. A Review. *Prot. Met. Phys. Chem. Surf.* **2016**, *52*, 254–266. [CrossRef]
52. Vinokurov, E.G.; Arsenkin, A.M.; Grigorovich, K.V.; Bondar, V.V. The Structure of the Chromium Coatings Modified by the Dispersed Particles. *Prot. Met.* **2006**, *42*, 204–207. [CrossRef]
53. Kazmanli, M.K.; Ürgen, M.; Cakir, A.F. Effect of nitrogen pressure, bias voltage and substrate temperature on the phase structure of Mo-N coatings produced by cathodic arc PVD. *Surf. Coat. Technol.* **2003**, *167*, 77–82. [CrossRef]
54. Postolnyi, B.O.; Beresnev, V.M.; Abadias, G.; Bondar, O.V.; Rebouta, L.; Araujo, J.P.; Pogrebnjak, A.D. Multilayer design of CrN/MoN protective coatings for enhanced hardness and toughness. *J. Alloy Compd.* **2017**, *725*, 1188–1198. [CrossRef]
55. Beresnev, V.M.; Klimenko, S.A.; Sobol', O.V.; Grankin, S.S.; Stolbovoi, V.A.; Turbin, P.V.; Novikov, V.Y.; Meilekhov, A.A.; Litovchenko, S.V.; Malikova, L.V. Effect of the Deposition Parameters on the Phase-Structure State, Hardness, and Tribological Characteristics of Mo_2N/CrN Vacuum-Arc Multilayer Coatings. *J. Superhard Mater.* **2016**, *38*, 114–122. [CrossRef]
56. Dolmatov, V.Y.; Lapchuk, N.M.; Lapchuk, T.M.; Nguyen, B.T.T.; Myllymäki, V.; Vehanen, A.; Yakovlev, R.Y. A Study of Defects and Impurities in Doped Detonation Nanodiamonds by EPR, Raman Scattering, and XRD Methods. *J. Superhard Mater.* **2016**, *38*, 219–229. [CrossRef]
57. Druz, B.; Zaritskiy, I.; Yevtukhov, Y.; Konchits, A.; Valakh, M.; Shanina, B.; Kolesnik, S.; Yanchuk, I.; Gromovoy, Y. Diamond-like carbon films: Electron spin resonance (EPR) and Raman spectroscopy. *Diam. Relat. Mater.* **2004**, *13*, 1592–1602. [CrossRef]
58. Wu, K.; Wu, B.; Li, C.; Hu, X. Gradation, Dispersion, and Tribological Behaviors of Nanometric Diamond Particles in Lubricating Oils. In *Introduction to Mechanical Engineering*; Paulo Davim, J., Ed.; Springer International Publishing AG, part of Springer Nature: Cham, Switzerland, 2018; pp. 120–128.
59. Sun, K.W.; Wang, C.Y. Optical properties of a single free standing nanodiamond. *J. Phys. Conf. Ser.* **2007**, *92*, 012031. [CrossRef]
60. Othman, M.F.; Bushroa, A.R.; Abdullah, W.N.R. Evaluation techniques and improvements of adhesion strength for TiN coating in tool applications: A review. *J. Adhes. Sci. Technol.* **2015**, *29*, 569–591. [CrossRef]
61. Komiyama, S.; Sutou, Y.; Oikawa, K.; Koike, J.; Wang, M.; Sakurai, M. Wear and oxidation behavior of reactive sputtered δ-(Ti,Mo)N films deposited at different nitrogen gas flow rates. *Tribol. Int.* **2015**, *87*, 32–39. [CrossRef]
62. Matei, A.A.; Pencea, I.; Stanciu, S.G.; Hristu, R.; Antoniac, I.; Ciovica, E.; Sfat, C.E.; Stanciu, G.A. Structural characterization and adhesion appraisal of TiN and TiCN coatings deposited by CAE-PVD technique on a new carbide composite cutting tool. *J. Adhes. Sci. Technol.* **2015**, *29*, 2576–2589. [CrossRef]
63. Kim, H.K.; La, J.H.; Kim, K.S.; Lee, S.Y. The effects of the H/E ratio of various Cr–N interlayers on the adhesion strength of CrZrN coatings on tungsten carbide substrates. *Surf. Coat. Technol.* **2015**, *284*, 230–234. [CrossRef]